



OPEN

Role of additional PCBM layer between ZnO and photoactive layers in inverted bulk-heterojunction solar cells

SUBJECT AREAS:
ELECTRONIC DEVICES
APPLIED PHYSICSReceived
23 October 2013Accepted
17 February 2014Published
7 March 2014Correspondence and
requests for materials
should be addressed to
S.C. (sucho@ulsan.ac.
kr); D.C.L. (dclim@
kims.re.kr) or Y.D.K.
(ydkim91@skku.edu)Shinuk Cho¹, Kwang-Dae Kim², Jinhee Heo³, Joo Yul Lee³, Gihoon Cha³, Bo Yeol Seo³, Young Dok Kim², Yong Soo Kim¹, Si-young Choi³ & Dong Chan Lim³¹Department of Physics and Energy Harvest Storage Research Center, University of Ulsan, Ulsan 680-749 (Republic of Korea),²Department of Chemistry, Sungkyunkwan University, Suwon 440-746 (Republic of Korea), ³Surface Technology Division, Korea Institute of Materials Science, Changwon 641-010 (Republic of Korea).

In order to induce greater light absorption, nano-patterning is often applied to the metal-oxide buffer layer in inverted bulk-heterojunction (BHJ) solar cells. However, current homogeneity was significantly disturbed at the interface, leading to an efficiency that was not fully optimized. In this work, an additional PC₆₁BM layer was inserted between the ZnO ripple and the photoactive layer to enhance the electron extraction. The insertion of additional PC₆₁BM layer provided substantial advantages in the operation of inverted BHJ solar cells; specifically, it enhanced current homogeneity and lowered accumulation and trapping of photogenerated charges at the ZnO interface. Inclusion of the additional PC₆₁BM layer led to effective quenching of electron-hole recombination by a reduction in the number of accumulated charges at the surface of ZnO ripples. This resulted in a 16% increase in the efficiency of inverted BHJ solar cells to 7.7%, compared to solar cells without the additional PC₆₁BM layer.

Bulk heterojunction (BHJ) solar cells based on blends of conjugated polymers and soluble fullerene derivatives have generated strong interest in the field of renewable energy because of the potential they offer to lower manufacturing costs for large area, lightweight devices^{1–3}. Since the first BHJ solar cell was reported in 1995^{4,5}, the power conversion efficiency (PCE) of BHJ solar cells has gradually improved due to the development of new materials and device architectures, recently reaching over 9% in single junction device^{6–8}.

The inverted device architecture in particular has gained considerable attention in the research community because of its better device stability and advantages in processing over the conventional architecture^{9–14}. In the inverted structure, since the polarity of charge collection is the opposite of that in the conventional architecture; the selection of an effective electron extraction/transportation buffer layer, which can effectively build-up the symmetry breaking, is the key component for high performance inverted solar cells^{15,16}. Such an electron extraction/transportation buffer layer must be highly transparent, electrically conductive, and energetically well-matched to the lowest unoccupied molecular orbital (LUMO) level of the acceptor.

In order to induce greater light absorption in the photoactive layer, nano-patterning is often applied to the metal-oxide buffer layer, which functions as the electron extraction/transportation layer. Not only on metal-oxide buffer layer, plasticizer assisted soft embossing (PASE) structure have been applied on PEDOT:PSS hole extracting layer to improve solar cell performance¹⁷. For P3HT:PCBM solar cells based on PASE structured PEDOT:PSS layers the averaged overall power efficiency is improved by up to 18%. Many demonstrations of successful PCE enhancement through improved charge extraction and light absorption due to light scattered by the imprinted patterns have been reported to-date^{18–21}. However, in most cases, the nano-patterning process is not simple, normally requiring the addition of complex fabrication steps.

Recently, we have demonstrated a simple method for spontaneous formation of nano-ripple structures on ZnO thin films fabricated using a sol-gel process; these nano-structured ZnO films were used as the hole-blocking, electron-transporting layer in inverted organic solar cells^{22,23,25,26}. Although the ZnO ripple structure delivered some enhancement of light absorption via light scattering, current homogeneity was significantly disturbed at the interface between the photoactive and ZnO layers, leading to a PCE that was not fully optimized. This current inhomogeneity problem was resolved in our previous work by the application of an ultra-thin pure ZnO layer with atomic layer deposition (ALD)^{23,24}. Although current technology allows the ALD processing on roll-to-roll



process under near atmosphere pressure, ALD is still not a simple technique so far; rather, it requires complicates equipment and additional processing steps.

In this work, rather than deposition of an ultra-thin ZnO layer with ALD, we have applied an additional electron transporting layer of phenyl-C61-butyric acid methyl ester (PC₆₁BM) by a simple spin-coating method. Inverted BHJ solar cells fabricated using poly (thienothiophene-co-benzodithiophenes)-7-F20 (PTB7-F20) and phenyl-C71-butyric acid methyl ester (PC₇₁BM) using the additional PC₆₁BM layer exhibited a 16% increase in PCE (to 7.7%) compared to solar cells without the additional PC₆₁BM layer (6.5%), which is consistent with previous literatures^{25,26}. Current-sensing atomic force microscopy measurements and photoexcitation-assisted capacitance-voltage measurements were then used to investigate the exact role of the additional PC₆₁BM layer on top of the ZnO ripple structure.

Results

Figure 1 shows a schematic illustration of the inverted solar cell structure as well as the chemical structures of the photoactive layer materials. After deposition of the solution-prepared ZnO on cleaned indium tin oxide (ITO)-coated glass by spin-coating under atmospheric conditions, a self-organized ripple nanostructure was introduced to enhance light absorption. Detailed procedures of the development of the ZnO nanostructures are described elsewhere^{22,23,27}. Figure 2c shows the TEM cross-section image of the device with PC₆₁BM layer. Since the ZnO and PCBM both showed dark phase in TEM image, it is somewhat difficult to distinguish. However, we thought that slight change of contrast from dark gray to light gray indicated PCBM layer. From the TEM image, we suspected that the thickness of PCBM layer is ca. 5 nm. This value was consistent with the result obtained from the comparison of total thickness between ITO/ZnO ripple/Active layer sample and ITO/ZnO ripple/PCBM/Active layer sample.

Figure 2a and 2c show AFM images of ZnO ripple structures with a mean height of ~47 nm. Surface morphology images of ZnO ripples after spin-coating PC₆₁BM on top is shown in Fig. 2b and 2d. Although the ripple nanostructures themselves were not significantly

changed, the PC₆₁BM coat was clearly distinguishable between crests. The root mean square (RMS) roughness was also reduced from 47.3 nm to 30.2 nm after the PC₆₁BM spin-coating.

A more interesting effect of the additional PC₆₁BM layer was observed in current-sensing AFM images shown in Fig. 2e and 2f. The current mapping image obtained from the ZnO ripple without PC₆₁BM exhibits inhomogeneous current levels. The ripple nanostructure of ZnO can be seen quite clearly. However, in the current mapping image obtained from the ZnO layer with PC₆₁BM, the ripple nanostructure shape largely disappeared, showing a relatively homogeneous current level across the image.

Such a current homogeneity has a critical effect on the BHJ solar cell performance. Figure 3a shows the current density (*J*)-voltage (*V*) characteristics of inverted PTB7-F20:PC₇₁BM solar cells with and without PC₆₁BM on the ZnO ripple. The solar cells fabricated without a PC₆₁BM layer yielded a PCE of 6.475%, with a short circuit current density (*J*_{sc}) of 14.783 mA/cm², an open circuit voltage (*V*_{oc}) of 0.693 V, and a fill factor (FF) of 0.631. The solar cells including PC₆₁BM, yielded a significantly enhanced PCE of 7.698%, with *J*_{sc} = 17.042 mA/cm², *V*_{oc} = 0.684 V, and FF = 0.660. Details related to the performance of the solar cells are listed in Table 1. A direct comparison of the *J*-*V* curves of the solar cells with and without the PC₆₁BM layer clearly indicate that the enhanced PCE in the devices with PC₆₁BM is largely based on an improvement of *J*_{sc}^{25,26}. We attributed the increase in *J*_{sc} to the improved current homogeneity at the interface between the ZnO ripples and the photoactive layer. Addition of PC₆₁BM layer on non-rippled ZnO layer also induced PCE enhancement. However, the PCE enhancement in device with non-rippled ZnO layer is originated from the *V*_{oc} improvement (see Figure S5 in supporting information). Note that the PCE enhancement in device with ZnO ripple was based on the improvement of *J*_{sc}. In non-rippled ZnO case, we suspected that there is a certain energy level modification of ZnO surface; maybe different band bending properties at the interface of non-rippled ZnO layer.

Figure 3b shows the external quantum efficiency (EQE) spectra for the inverted PTB7-F20:PC₇₁BM solar cells with and without the PC₆₁BM layer. The overall EQE spectrum of solar cell with PC₆₁BM

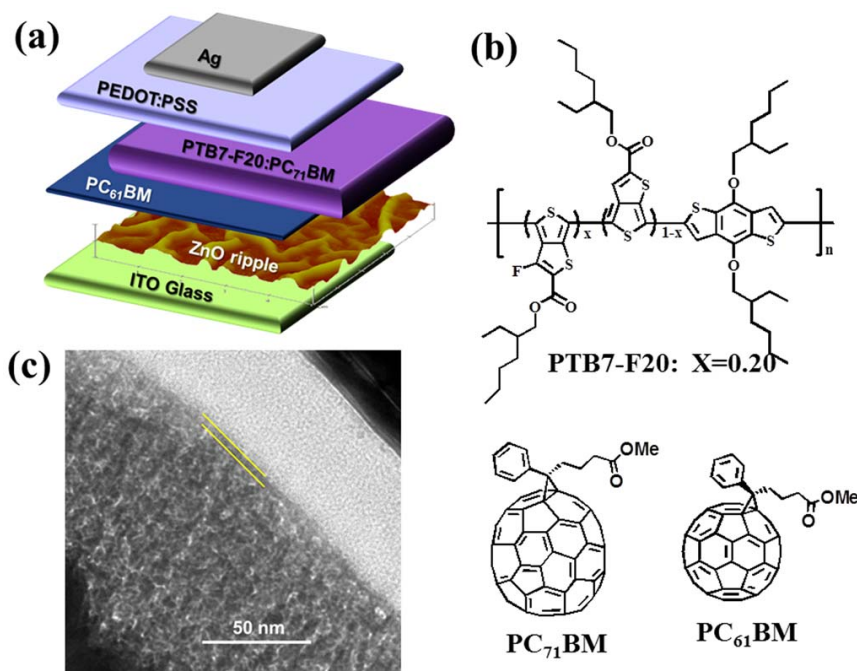


Figure 1 | (a) Schematic illustration of an inverted solar cell structure and (b) chemical structures of the photoactive materials. (c) Cross section TEM image of the inverted BHJ solar cells with additional PC₆₁BM layer.

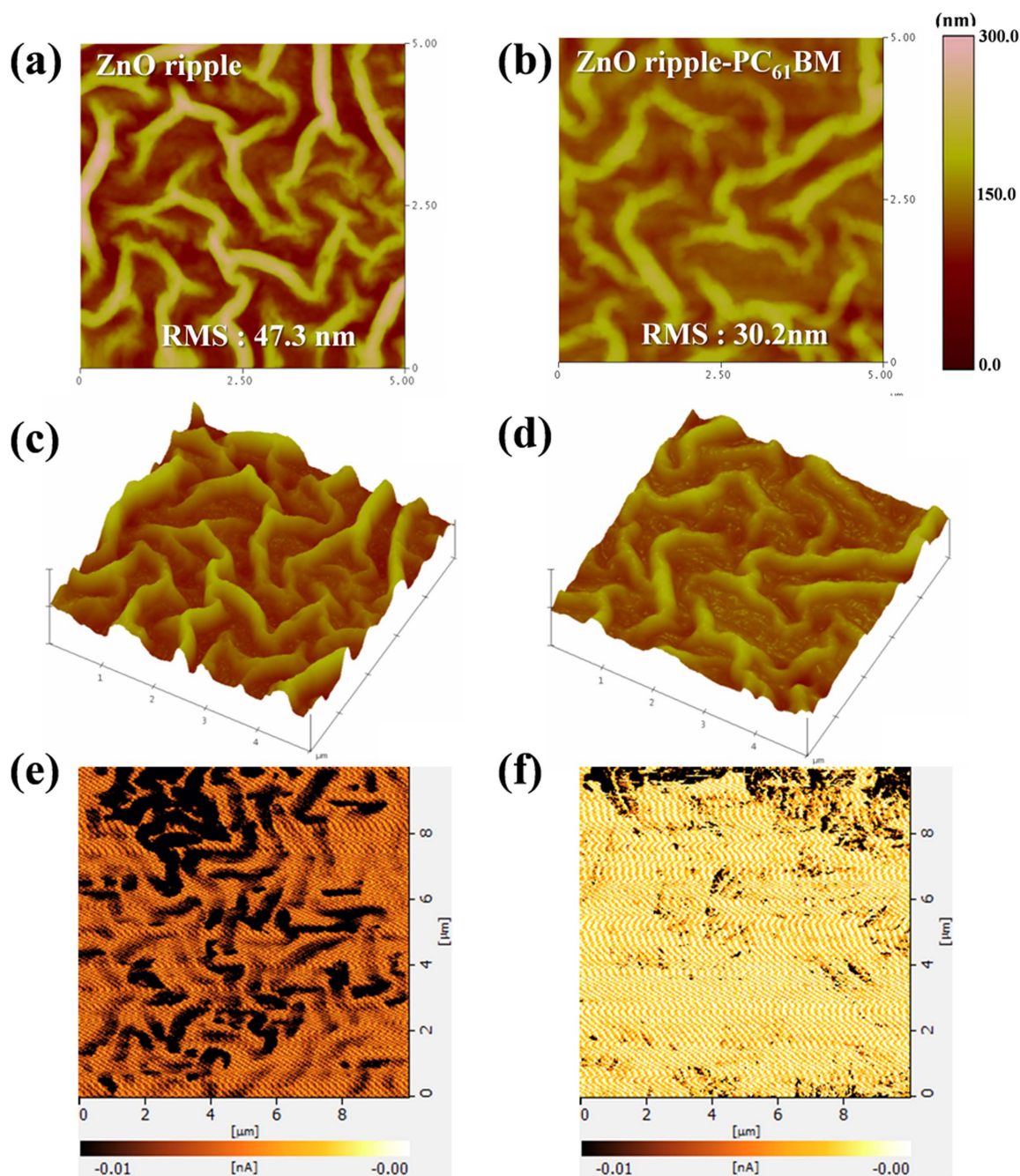


Figure 2 | AFM height images of ZnO ripple structures (a) without and (b) with PC₆₁BM. 3D AFM image of ZnO ripple structures (c) without and (d) with PC₆₁BM. Current-sensing AFM images of ZnO ripple structures (e) without and (f) with PC₆₁BM. Note that the current value in scale bar is individually normalized value to comparison.

was slightly higher than that of the solar cell without it. Particularly, increase in EQE spectrum is occurred in entire wave range. It indicates that EQE enhancement is most likely due to the transport properties change, not because of optical property change by addition of PC₆₁BM layer. The J_{sc} difference between the devices with and without PC₆₁BM is consistent with the value derived from the EQE spectra.

In general, J_{sc} can also be strongly influenced by interfacial charge trapping at the metal oxide interface. Photoexcitation-assisted capacitance voltage (CV) spectroscopy was conducted to investigate the additional effect of the PC₆₁BM layer on interfacial charge trapping and accumulation. Figure 4 shows the CV characteristics for devices both with and without the PC₆₁BM layer at various photo-excitation intensities between 20 and 100 mW/cm². In both sets of CV spectra,

the effective capacitance increased with increasing photoexcitation intensity because effective capacitance under illumination is directly related to the density of photo generated charge²⁸.

Additionally, the voltage value at maximum capacitance (V_{C-max}) shifted to a slightly lower voltage. V_{C-max} generally corresponds to the voltage at which the charge carriers begin to inject, neutralizing the photo-generated charge, thereby decreasing the capacitance value (See supporting information, figure S5)²⁹. Accordingly, V_{C-max} should be reduced if the photo-generated charges accumulate at the metal oxide interface. In addition, the degree of V_{C-max} shift will be proportional to the amount of accumulated charge. The observed V_{C-max} shift was 0.108 V for the solar cells without a PC₆₁BM layer (Figure 4a), while the solar cells with a PC₆₁BM layer exhibited a much smaller V_{C-max} shift of 0.057 V (Figure 4b).

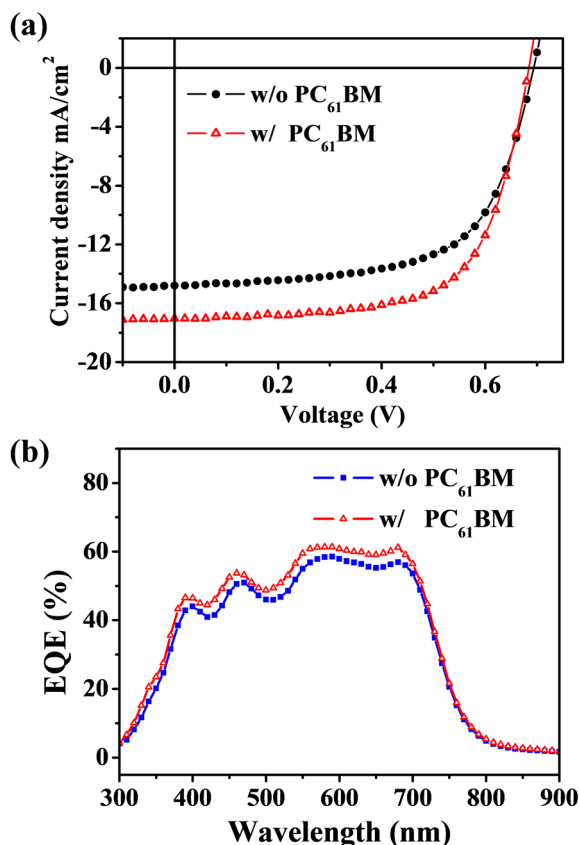


Figure 3 | (a) J - V characteristics of inverted PTB7-F20:PC₇₁BM solar cells with and without PC₆₁BM on the ZnO ripple, (b) EQE spectra of the inverted PTB7-F20:PC₇₁BM solar cells with and without the PC₆₁BM layer.

Therefore, comparison of the V_{C-max} shifts between the solar cells with and without a PC₆₁BM layer indicates that the solar cell with a PC₆₁BM layer has a lesser accumulation of photo-generated charge at the interface. In other words, the additional PC₆₁BM layer effectively prevented the trapping of charge at the surface of the ZnO ripples, thereby leading to better charge extraction.

In BHJ solar cells, non-geminate recombination via interfacial states, which exist at the donor-acceptor interface, is one of the dominant loss mechanisms^{30–32}. Such non-geminate band-to-band recombination can also occur at the metal oxide-photoactive layer interface³². Impedance spectroscopy was used on inverted PTB7-F20:PC₇₁BM solar cells both with and without a PC₆₁BM layer on top of the ZnO ripple to clarify the dynamics of charge transport and recombination at the ZnO ripple surface. Figure 5 shows intensity-modulated photocurrent spectroscopy (IMPS) and intensity-modulated photovoltage spectroscopy (IMVS) results obtained under illumination with a narrow-band red LED light (635 nm). Note that 635 nm light is in the polymer absorption region. For the solar cells without a PC₆₁BM layer, calculated transit time (τ_t , from IMPS) and recombination time (τ_r , from IMVS) were 64.4 and 120.9 μ s, respectively^{29,31,33–35}. For the solar cells with a PC₆₁BM layer, τ_t and τ_r were calculated as 76.4 and 438.1 μ s, respectively.

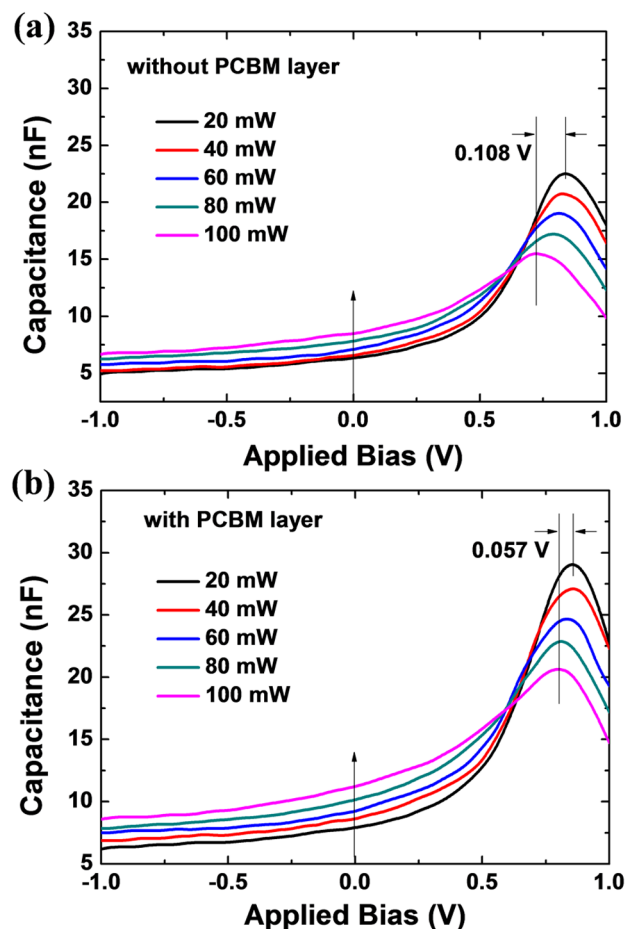


Figure 4 | Photo-assisted capacitance-voltage characteristics at various photo-excitation intensities from 20 to 100 mW/cm² (a) for the inverted PTB7-F20:PC₇₁BM solar cells without a PC₆₁BM layer and (b) for solar cells with a PC₆₁BM layer.

Charge collection efficiencies (η_c) obtained via the relation $\eta_c = 1 - (\tau_t/\tau_r)$, were 46.7% for solar cells without a PC₆₁BM layer and 82.6% for solar cells with one³⁶. These results are consistent with the results obtained from CV spectroscopy. Slower recombination time and enhanced charge collection efficiency in the solar cells with a PC₆₁BM layer can be explained by the extra layer effectively covering trap sites and allowing less accumulation of photoexcited charges at the ZnO interface.

In summary, we have demonstrated high performance inverted BHJ solar cells with PCEs enhanced by the insertion of an additional PC₆₁BM layer between the self-organized, rippled ZnO and photoactive layers. Inverted BHJ solar cells including a PC₆₁BM layer exhibited PCEs of 7.7%, nearly 16% higher than those of solar cells without an additional PC₆₁BM layer. Insertion of an additional PC₆₁BM layer provided substantial dynamic advantages in the operation of inverted BHJ solar cells. First, current-sensing AFM showed that the additional PC₆₁BM layer clearly improved current homogeneity at the ZnO ripple-photoactive layer interface. Secondly, photo-excitation-assisted CV measurements indicated

Table 1 | Photovoltaic performance of the inverted PTB7-F20:PC₇₁BM solar cells with and without a PC₆₁BM layer

PTB7-F20:PC ₇₁ BM Inverted solar cells	PCE [%]	FF	V_{oc} [V]	J_{sc} [mA/cm ²]	R_s [Ω ·cm ²]
w/o PC ₆₁ BM	6.475	0.631	0.693	14.783	2.924
w/PC ₆₁ BM	7.698	0.660	0.684	17.042	2.149

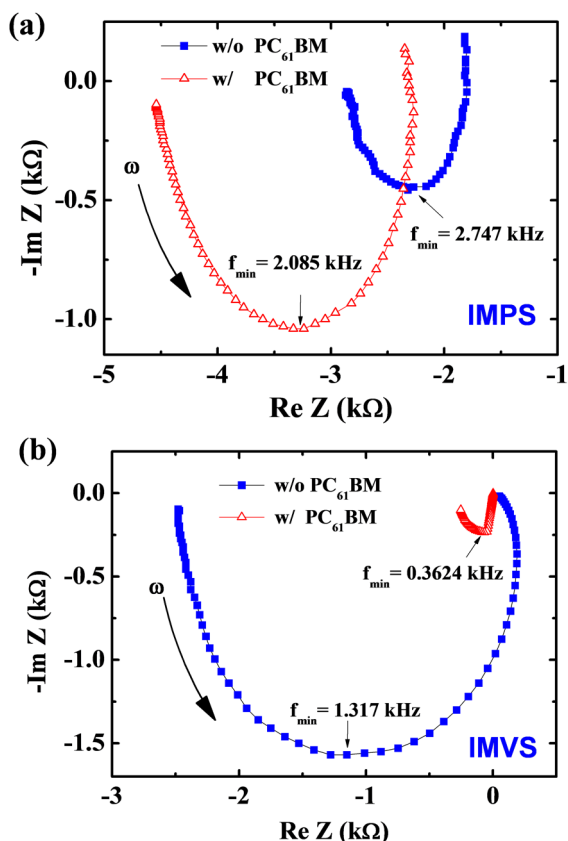


Figure 5 | Nyquist plot of (a) IMPS and (b) IMPS results. Narrow-band red LED light (635 nm) was used for the AC and DC components of the illumination. The mean transit time (τ_t) of photogenerated charges and recombination time (τ_r) were obtained at the frequency minimum in the Nyquist plot of IMVS and IMPS results.

that the solar cells with a PC_{61}BM layer accumulate and trap fewer photo-generated charges at the interface. IMPS and IMVS studies also clearly showed slower recombination time and enhanced charge collection efficiency in the solar cells with a PC_{61}BM layer. We therefore concluded that the enhanced PCE in solar cells with a PC_{61}BM layer was attributed to effective quenching of electron-hole recombination by reducing accumulated (or trapped) charges at the surface of the ZnO ripples.

Methods

Preparation of ZnO sol-gel. ZnO sol-gel solution (concentration of solution; 0.75 M) was prepared by dissolving zinc acetate [$\text{Zn}(\text{CH}_3\text{COO})_2 \cdot 2\text{H}_2\text{O}$] (Aldrich, 99.99%) in 2-methoxyethanol (Aldrich, 99.8%) containing ethanolamine as a stabilizer. The solution was kept stirring for 2–3 h at 60 °C using a magnetic stirrer to obtain a homogeneous solution.

Conductive AFM measurement. Conductive atomic force microscopy (C-AFM, Seiko E-Sweep) was conducted for evaluating the surface current flow in the films. For current images of the films, contact mode and tips with Pt/Ir were chosen.

Fabrication of inverted solar cells. Inverted solar cells studied in the present work consisted of a stack of ITO-coated glass/ZnO nano-ripple film with or without PC_{61}BM layer/BHJ photoactive layer/PEDOT : PSS/Ag. ITO-coated glass substrates ($4 \Omega/\square$, $2.5 \times 2.5 \text{ cm}^2$) were first cleaned by ultrasonic agitation in detergent, deionized water, acetone, and isopropanol in sequence, followed by drying at 100 °C in an oven for an hour and then UV ozone treatment for 30 min. 160 μl of ZnO solution was spin-coated on top of the pre-cleaned ITO glass at 2000 rpm for 40 sec. After coating, ZnO films were annealed at a constant heating rate of 22 °C/min from room temperature up to 350 °C to make a ZnO-ripple structure. The PC_{61}BM was dissolved in chlorobenzene (CB) at a concentration of 1.0 wt%. The PC_{61}BM solution was spin-cast on top of the ZnO-ripple film at a speed of 1000 rpm for 40 sec. The BHJ photoactive layers were spin cast at a speed of 1000 rpm for 40 sec in a N_2 -filled glove box from a solution of PTB7-F20 : PC_{71}BM (8 mg : 12 mg) in CB with 3 v/v% 1,8-diiodooctane (DIO) that was first passed through a 0.20 μm

polytetrafluoroethylene (PTFE) filter. To avoid washing out or mixing during the upper layer spin-coating, the lower PC_{61}BM layer was covered with an orthogonal solvent, ethanol, by spin coating at 1500 rpm for 5 s, followed immediately by the upper layer of PTB7-F20 : PC_{71}BM . The coated films were annealed at 80 °C for 10 min to evaporate residual solvent. After deposition of the photoactive layer, PEDOT : PSS (Clevios P VP AI 4083, Heraeus), diluted in isopropyl alcohol (in a 1 : 10 ratio) was spin-coated on top of the photoactive layer at 5000 rpm for 60 sec in a glovebox. It is worth emphasizing that no post annealing of PEDOT : PSS layers was performed. Finally, an Ag top electrode (100 nm) was deposited by thermal evaporation at 3×10^{-6} Torr using a shadow mask to form an active area of 0.38 cm^2 .

Characterization of solar cells. The current density–voltage (J - V) characteristics of the solar cell devices were measured using a PEC-L11 model 13 (Pecell Technologies Inc.) under simulated AM 1.5 illumination at an intensity of 100 mW/cm^2 . The intensity of sunlight illumination was calibrated using a standard Si-photodiode detector with a KG-5 filter. External quantum efficiency (EQE) spectra of each solar cell were measured using a solar cell spectral response/QE/IPCE measurement system (Newport co., Oriel IQE-200TM).

IMPS, IMVS and CV measurements. Photoexcitation-assisted CV measurements were carried out using HP4194 impedance analyzer under illumination at various intensity of 20 ~ 100 mW/cm^2 . IMPS and IMVS were carried out using an impedance analyzer (IVIUM Tech., IviumStat). Both DC and AC components of the illumination were provided by the red emission LED ($\lambda = 635 \text{ nm}$). The modulation depth of the AC component superimposed on the DC light was 10%. The light intensity was 0.86 mW/cm^2 , measured using a silicon photodiode. IMPS and IMVS were obtained under short-circuit and open-circuit conditions, respectively. The mean transit time (τ_t) and recombination time (τ_r) of photogenerated charges were obtained from the frequency minimum in the Nyquist plot of IMVS and IMPS results by setting $\tau_{\text{rt}} = (2\pi f_{\text{min}} (\text{IMVS}, \text{IMPS}))^{-1}$.

- Thompson, B. C. & Fréchet, J. M. J. Polymer-fullerene composite solar cells. *Angew. Chem. Int. Ed.* **47**, 58–77 (2008).
- Brabec, C. J. *et al.* Polymer–fullerene bulk-heterojunction solar cells. *Adv. Mater.* **22**, 3839–3856 (2010).
- Peet, J., Senatore, M. L., Heeger, A. J. & Bazan, G. C. The role of processing in the fabrication and optimization of plastic solar cells. *Adv. Mater.* **21**, 1521–1527 (2009).
- Yu, G., Hummelen, J., Wudl, F. & Heeger, A. J. Polymer Photovoltaic Cells: Enhanced Efficiencies via a Network of Internal Donor-Acceptor Heterojunctions. *Science* **270**, 1789–1791 (1995).
- Halls, J. J. M. *et al.* Efficient photodiodes from interpenetrating polymer networks. *Nature* **376**, 498–500 (1995).
- He, Z. *et al.* Enhanced power-conversion efficiency in polymer solar cells using an inverted device structure. *Nat. Photonics* **6**, 591–595 (2012).
- Cabanetos, C. *et al.* Linear side chains in benzo[1,2-b:4,5-b']dithiophene-thieno[3,4-c]pyrrole-4,6-dione polymers direct self-assembly and solar cell performance. *J. Am. Chem. Soc.* **135**, 4656–4659 (2013).
- Dou, L. *et al.* Tandem polymer solar cells featuring a spectrally matched low-bandgap polymer. *Nat. Photonics* **6**, 180–185 (2012).
- Liao, H.-H., Chen, L.-M., Xu, Z., Li, G. & Yang, Y. Highly efficient inverted polymer solar cell by low temperature annealing of Cs_2CO_3 interlayer. *Appl. Phys. Lett.* **92**, 173303 (2008).
- White, M. S., Olson, D. C., Shaheen, S. E., Kopidakis, N. & Ginley, D. S. Inverted bulk-heterojunction organic photovoltaic device using a solution-derived ZnO underlayer. *Appl. Phys. Lett.* **89**, 143517 (2006).
- Waldauf, C. *et al.* Highly efficient inverted organic photovoltaics using solution based titanium oxide as electron selective contact. *Appl. Phys. Lett.* **89**, 233517 (2006).
- Jørgensen, M. *et al.* Stability of polymer solar cells. *Adv. Mater.* **24**, 580–612 (2012).
- Shim, W. H. *et al.* Multifunctional SWCNT-ZnO nanocomposites for enhancing performance and stability of organic solar cells. *Adv. Mater.* **23**, 519–522 (2011).
- Savva, A. *et al.* The effect of organic and metal oxide interfacial layers on the performance of inverted organic photovoltaics. *Adv. Energy Mat.* **3**, 391–398 (2013).
- Motiei, L. *et al.* Self-propagating molecular assemblies as interlayers for efficient inverted bulk-heterojunction solar cells. *J. Am. Chem. Soc.* **132**, 12528–12530 (2010).
- Seo, J. H., Kim, H. & Cho, S. Build-up of symmetry breaking using a titanium suboxide in bulk-heterojunction solar cells. *Phys. Chem. Chem. Phys.* **14**, 4062–4065 (2012).
- Meier, R., Birkenstock, C., Palumbiny, C. M. & Müller-Buschbaum, P. Efficiency-improved organic solar cells based on plasticizer assisted soft embossed PEDOT : PSS layers. *Phys. Chem. Chem. Phys.* **14**, 15088–15098 (2012).
- Emah, J. B., Curry, R. J. & Silva, S. R. P. Low cost patterning of poly(3,4-ethylenedioxythiophene) poly(styrenesulfonate) films to increase organic photovoltaic device efficiency. *Appl. Phys. Lett.* **93**, 103301 (2008).
- Wang, D. H. *et al.* Effect of the ordered 2D-dot nano-patterned anode for polymer solar cells. *Org. Electron.* **11**, 285–290 (2010).



20. Wang, D. H., Seifert, J., Park, J. H., Choi, D.-G. & Heeger, A. J. Efficiency increase in flexible bulk heterojunction solar cells with a nano-patterned indium zinc oxide anode. *Adv. Energy Mater.* **2**, 1319–1322 (2012).
21. Kang, M.-G., Kim, M.-S., Kim, J. & Guo, L. J. Organic solar cells using nanoimprinted transparent metal electrodes. *Adv. Mater.* **20**, 4408–4413 (2008).
22. Lim, D. C. *et al.* Spontaneous formation of nanoripples on the surface of ZnO thin films as hole-blocking layer of inverted organic solar cells. *Sol. Energy Mater. Sol. Cells* **95**, 3036–3040 (2011).
23. Lim, D. C. *et al.* Towards fabrication of high-performing organic photovoltaics: new donorpolymer, atomic layer deposited thin buffer layer and plasmonic effects. *Energy Environ. Sci.* **5**, 9803–9807 (2012).
24. Kim, K.-D. *et al.* Surface modification of a ZnO electron-collecting layer using atomic layer deposition to fabricate high-performing inverted organic photovoltaics. *ACS Appl. Mater. Interfaces* **5**, 8718–8723 (2013).
25. Hsieh, C.-H. *et al.* Highly Efficient and Stable Inverted Polymer Solar Cells Integrated with a Cross-Linked Fullerene Material as an Interlayer. *J. Am. Chem. Soc.* **132**, 4887–4893 (2010).
26. Cheng, Y.-J., Hsieh, C.-H., He, Y., Hsu, C.-S. & Li, Y. Combination of Indene-C60 Bis-Adduct and Cross-Linked Fullerene Interlayer Leading to Highly Efficient Inverted Polymer Solar Cells. *J. Am. Chem. Soc.* **132**, 17381–17383 (2010).
27. Park, H.-Y., Lim, D., Kim, K.-D. & Jang, S.-Y. Performance optimization of low-temperature-annealed solution-processable ZnO buffer layers for inverted polymer solar cells. *J. Mater. Chem. A* **1**, 6327–6334 (2013).
28. Boix, P. P., Wienk, M. M., Janssen, R. A. J. & Garcia-Belmonte, G. Open-circuit voltage limitation in low-bandgap diketopyrrolopyrrole-based polymer solar cells processed from different solvents. *J. Phys. Chem. C* **115**, 15075–15080 (2011).
29. Garcia-Belmonte, G. *et al.* Charge carrier mobility and lifetime of organic bulk heterojunctions analyzed by impedance spectroscopy. *Org. Electron.* **9**, 847–851 (2008).
30. Cowan, S. R., Street, E. A., Cho, S. & Heeger, A. J. Transient photoconductivity in polymer bulk heterojunction solar cells: Competition between sweep-out and recombination. *Phys. Rev. B* **83**, 035205 (2011).
31. Byers, J. C., Ballantyne, S., Rodionov, K., Mann, A. & Semenikhin, O. A. Mechanism of recombination losses in bulk heterojunction P3HT:PCBM solar cells studied using intensity modulated photocurrent spectroscopy. *ACS Appl. Mater. Interfaces* **3**, 392–401 (2011).
32. Tachibana, Y. *et al.* Organic conducting wire formation on a TiO₂ nanocrystalline structure: towards long-lived charge separated systems. *Chem. Commun.*, 4360–4362 (2009).
33. Fabregat-Santiago, F., Garcia-Belmonte, G., Mora-Seró, I. & Bisquert. Characterization of nanostructured hybrid and organic solar cells by impedance spectroscopy. *J. Phys. Chem. Chem. Phys.* **13**, 9083–9118 (2011).
34. Kavasoglu, N., Kavasoglu, A. S., Birgi, O. & Oktik, S. Intensity modulated short circuit current spectroscopy for solar cells. *Sol. Energy Mater. Sol. Cells* **95**, 727–730 (2011).
35. Bag, M. & Narayan, K. S. Universality in the intensity-modulated photocurrent in bulk-heterojunction polymer solar cells. *Phys. Rev. B* **82**, 075308 (2010).
36. Emin, S., Yanagida, M., Peng, W. & Han, L. Evaluation of carrier transport and recombinations in cadmium selenide quantum-dot-sensitized solar cells. *Sol. Energy Mater. Sol. Cells* **101**, 5–10 (2012).

Acknowledgments

This research was supported by a grant from KIMS. The portion of this research conducted at the University of Ulsan was supported by the Basic Science Research Program (NRF-2011-0009148, NRF-2013R1A2A2A01067741) and the Priority Research Centers Program (2009-0093818) through the National Research Foundation of Korea grant, funded by the Korean Government. Shinuk Cho and Kwang-Dae Kim contributed equally to this work.

Author contributions

S.C., D.C.L. and Y.D.K. conceived this project. K.D.K., G.C. and B.Y.S. designed and fabricated the solar cells. S.C. and Y.S.K. collected the data of photo-assisted CV measurements and IMPS, IMVS measurements. J.H. and J.Y.L. performed the conductive AFM experiments. S.C. wrote the manuscript, and all other authors contributed to the edits of the manuscript.

Additional information

Supplementary information accompanies this paper at <http://www.nature.com/scientificreports>

Competing financial interests: The authors declare no competing financial interests.

How to cite this article: Cho, S. *et al.* Role of additional PCBM layer between ZnO and photoactive layers in inverted bulk-heterojunction solar cells. *Sci. Rep.* **4**, 4306; DOI:10.1038/srep04306 (2014).



This work is licensed under a Creative Commons Attribution-NonCommercial-NoDerivs 3.0 Unported license. To view a copy of this license, visit <http://creativecommons.org/licenses/by-nc-nd/3.0>